LAWRENCE
LIVERMORE
NATIONAL
LABORATORY

LLNL-TH-416616

Time Integrated Soft X-ray Imaging in High Intensity Laser Experiments (thesis)

David Stafford

September 4, 2009

Disclaimer

This work performed under the auspices of the U.S. Department of Energy by Lawrence Livermore National Laboratory under Contract DE-AC52-07NA27344.

Time Integrated Soft X-ray Imaging in High Intensity Laser Experiments.
By

David Carl Stafford Student
B.S. (California State University Sacramento) 2006

Thesis

Submitted in partial satisfaction of the requirements for the degree of

MASTER OF SCIENCE

in

Applied Science

in the

OFFICE OF GRADUATE STUDIES

of the

UNIVERSITY OF CALIFORNIA

DAVIS

Approved:

_____(Professor Hector Baldis)

_____(Dr. Marilyn Schneider)

_____(Professor William Kruer)

Committee in Charge

2009

Acknowledgements

I would like to thank and acknowledge the following for their support and guidance throughout my research at the University of California at Davis (UCD) and LLNL. Dr. Hector Baldis (UCD) and Dr. Marilyn Schneider (LLNL) for allowing me into the High Temperature Hohlraum group, the Institute for Laser Science & Applications (ILSA) for their financial support, the entire staff at JLF for providing a state of the art student oriented laser research facility, and to Kelly Cone (UCD) and Lee Elberson (University of Maryland) for strong peer support.

Contents

Charts and Figures

Introduction

2009 marks a significant achievement and the dawn of a new era in high intensity laser research with the final commissioning of all 192 beams at the National Ignition Facility (NIF). NIF is a department of energy (DOE) funded project more than 10 years in the making located at the Lawrence Livermore National Laboratory (LLNL). The following research was done as one of many preliminary experiments done to prepare for these historic events.

The primary focus of the experimental campaign this paper addresses is to test and develop a thermal x-radiation source using a short pulse laser. This data is hoped to provide information about the thermal transport mechanisms important in the development of prediction models in High Energy Density (HED) science. One of several diagnostics fielded was a soft x-ray imager (SXRI) which is detailed in this paper. The SXRI will be used to measure the relative size of the heated region and also the relative level of specific x-ray emissions among several shot and target configurations.

The laser system used was the Titan laser located in the Jupiter Laser Facility (JLF) at Lawrence Livermore National Laboratory (LLNL). Titan uses the JLF Janus Nd:glass laser west frontend system with a Optical Parametric Chirped Pulse Amplification (OPCPA) in place of the nanosecond oscillator. The system is capable of producing laser intensities of over a petawatt with several tens of joules delivered in the beam.

SXRI

The soft x-ray imager (SXRI) was originally designed for early experiments at the National Ignition Facility (NIF) and ongoing experiments at Omega laser facility as a time resolved imager to study the burn through characteristics of high temperature hohlraum targets [1]. In three recent campaigns at Titan laser the SXRI was used as a time-integrated imager.

The SXRI in the time-integrated mode is a robust diagnostic. An image plate holder replaces the x-ray framing camera, which is the only part of the SXRI that is mechanically, or electronically controlled. This leaves is a simple pinhole camera imaging to a Fuji manufactured image plate. Only misalignment and clogged pinholes can cause problems with data collection. In the time-resolved configuration sixteen images are collected by an x-ray framing camera mated to the back of the SXRI body at the image plane. The images are arranged in a five by four configuration of rows and columns, the central column is only present if the magnification snout used is 3X or greater and is a straight through hard x-ray channel. Figure 1 is a typical scanned image from the SXRI. Each bright point is an image of the region of the target emitting the photons of specific energy bands as dictated by the mirrors

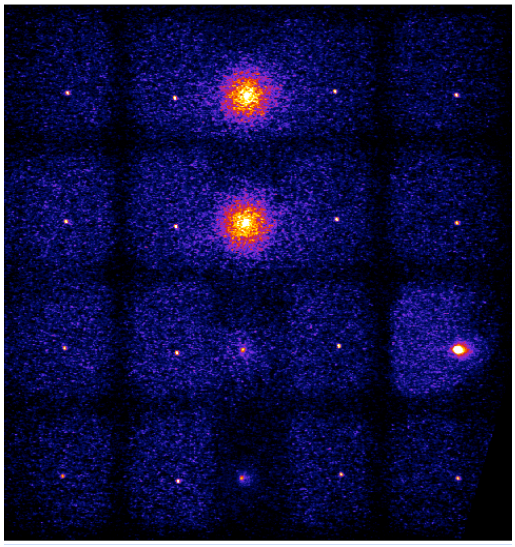

Figure 1: ImageJ picture of scanned image plate for a single shot

and filters of the diagnostic. The energy specified will be discussed later in this section. Twenty such spots are clearly visible. For ease of reference, the channels are numbered 1 to 20 as shown in figure 2.

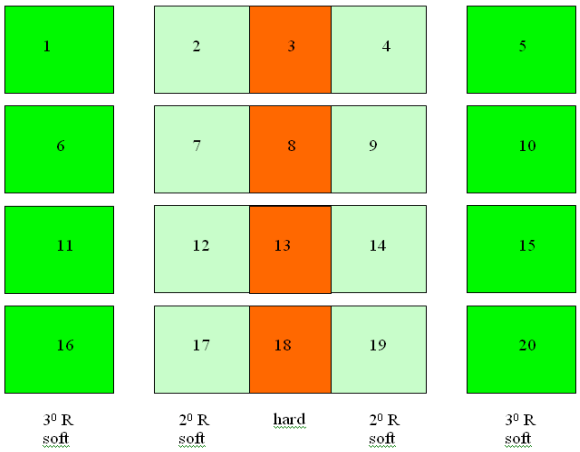

Figure 2: Channel numbering configuration.

The images are created by a combination of pinhole and glancing mirrors. Figure 3 is an illustration of the pinhole plate used in the most recent experimental campaign. The material used for the pinholes is 0.010” thick Tantalum (Ta), the holes are laser cut for high tolerance placement and clean edges. The pinhole plate is sandwiched between 0.011” Tungsten (W) plates, one closest to target chamber center (TCC) and two behind the pinhole plate. These W plates have 300μm holes cut to match the pinhole configuration and act as collimators [1]. Pinhole sizes are chosen based on calculations given by Lord Rayleigh and Josef Petzval [2] in the 19th century which equate the optimal pinhole size (*d*) to the focal plane distance from the pinhole (*f*), in this case the IP, and wavelength (λ) of the light given as;

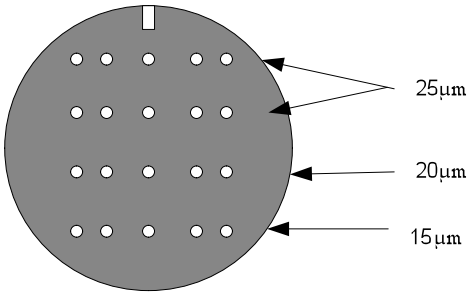

Figure 3: Changeable pinhole illustration.

$$d = 1.9\sqrt{f * \lambda}$$

Using Petzval's formula, we calculate the optimal pinhole to be 25μm where f = 23 inches (58.4cm) and = 1.6nm (≈ 750 eV, the central ROI from figure 6. The choice of smaller holes for the bottom rows was done for comparative studies.

Inside the body of the SXRI are two sets of matched mirrors, figure 4 is a top view of the SXRI. The pinholes are located at the front of the snout, left of the main body. The substrate for both sets of mirrors are 0.75” thick BK-7. The first

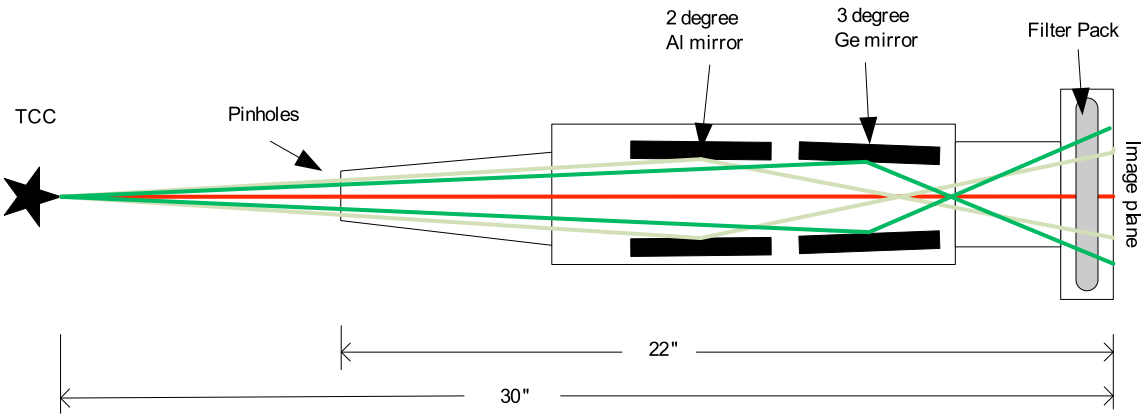

Figure 4: Cross section top view of SXRI. Image paths are shown.

set of mirrors, commonly referred to as the 2° channel, are coated with 1500 Å of Al and polished to 1 nm. The second set of mirrors, commonly referred to as the 3° channel, are coated with 1500 Å of Ge and polished to the same specifications. The actual glancing angles are given in the figure and were determined using the matter interaction tools as provided on the Center for X-ray Optics (CXRO) web site.

The filter pack is configured as shown in figure 5. The upper illustration is a face on view of the assembly as viewed from the target through the snout. The

lower illustration a cross section view of the layered filter captured between Al plates that have windows cut through. Note that the 100 and 200μm AL across the central channels are affixed to the outside of the cross section. This pack is versatile and easily reconfigured by adding or eliminating foils or other composite materials as determined by a specific region of interest in the electromagnetic spectrum.

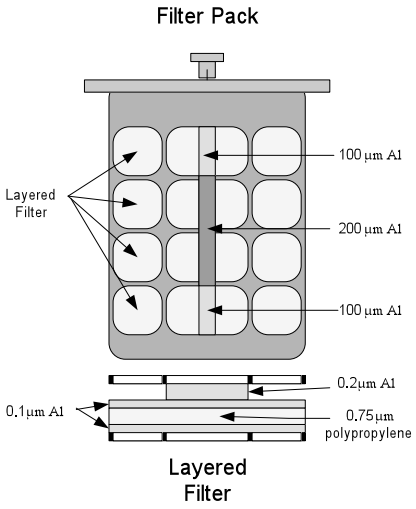

Figure 5: Removable filter pack.

Using a combination of foil filters and glancing mirrors it is possible to create moderate resolution “optical” notch filters for photons of any spectral bandwidth. This notch filter is the main feature of the SXRI. Any undergraduate electro-magnetism physics and electrical engineering circuits course will generally culminate in the exploration of band pass (notch) filters. In circuits, these filters are built by using a combination of capacitors and inductors, where the capacitor sets the high pass and the inductor the low pass filters. As an example, these filters are important in the tuning of a radio receiver to a specific signal frequency. The analogy of the optical notch filter to the electrical circuit band pass is that the foil acts as a high pass filter, where low energy photons are absorbed only allowing the high energy photons to pass. The glancing mirrors act as a low pass filter, where the lower energy photons are reflected and higher energy pass through the mirror. A detailed discussion of these processes are

found in many advanced solid state physics texts, this discussion is an synopsis of David Attwood's from his text Soft X-rays and Extreme Ultraviolet Radiation.

Due to the ultra-high intensity laser which is used in experiments involving the SXRI it is necessary to perform the experiments in a low vacuum environment ($<10^{-4}$ torr). Immediately, this simplifies the photon scattering zone, that is, the photons will pass from a vacuum into an isotropic solid material. There are then three basic reactions to consider, propagation through, refraction in, and reflection from the medium. Using the CXRO tools the transmission of photons can be displayed in charts (figure 6 and 7).

The heavy red line in fig. 6 indicate the region and percentage of transmission allowed by the mirror/filter combination for the 3^0 degree (outside columns). The majority of the emissions are ranging between 400 and 800 eV with the peak transmission at ~650 eV. The high pass as determined by the filter pack consisting of a plastic core (CH-N) sandwiched between thin foils as seen in figure 5. The plastic is represented by the green line figure 6, the CH-N allows transmission in the visible region, it is this region with the overlap of the low pass transmission that allows a small amount of transmission at the 200 eV x-ray energy.

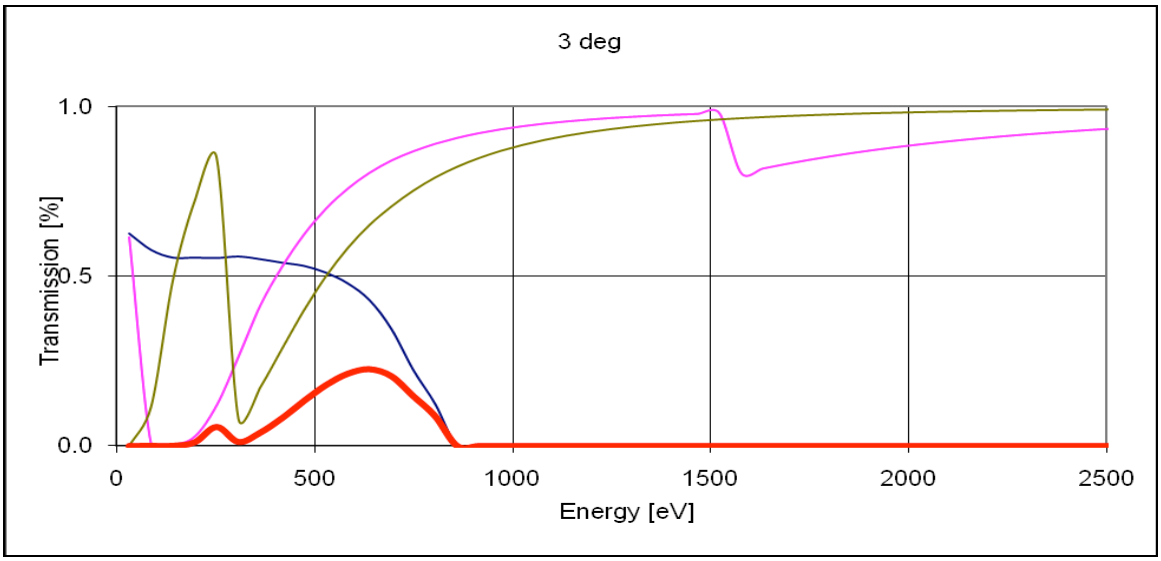

Figure 6: CXRO analysis of glancing mirror(blue line/low pass) and filter pack (pink and green line/high pass) and product of the combination (heavy red line) for soft x-ray emissions.

Figure 7 gives only the product of the filter pack with the additional thick Al foil attached to the framework of the pack. The low energy photons are completely blocked below 6k eV x-ray energy.

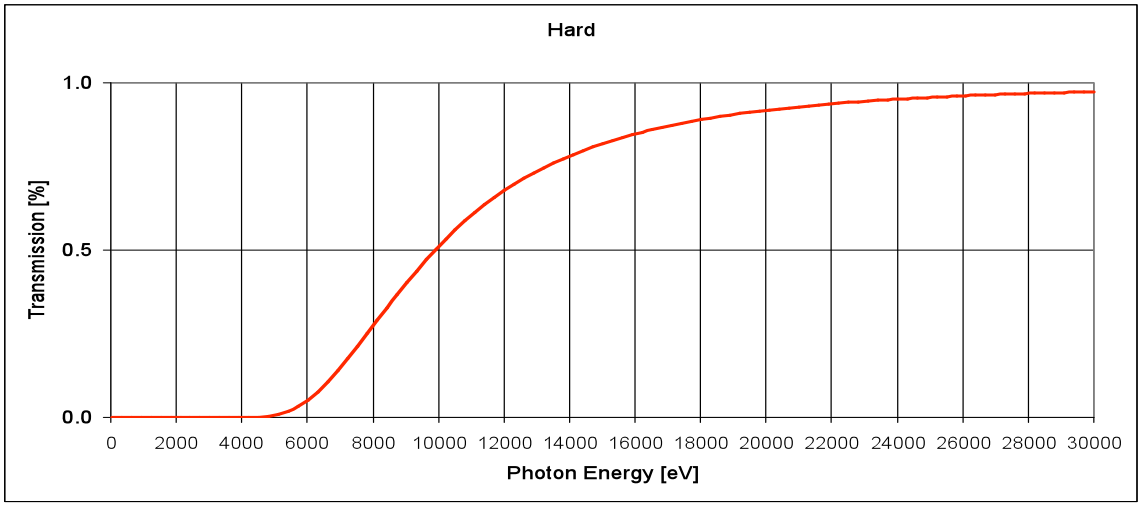

Figure 7: CXRO matter interaction chart for the high pass central channel.

The data was gather on Fuji BAS Image Plate (IP) type TR which is specifically designed with sensitivity in the 0-2keV spectral range [7]. The IP was scanned post shot exposure using a Fuji flatbed scanner model number FLA7000. The user settings used were: *Sensitivity*, S = s4000, *Latitude*, L = 5, and *Scan Resolution*, R = 25μm. The analysis was done using ImageJ, a shareware software program. Initially the values are given in greyscale (G) which gives the scaling of local photon intensity on the IP. ImageJ has a built in code to convert G to Photo Stimulated Luminescence (PSL) values. PSL units are proportional to the energy intensity within a given pixel processed by the scanner and provide a 2-dimenional image. The greyscale to PSL conversion [8,9] is given by:

$$PSL = \left(\frac{R}{100}\right)^2 \left(\frac{4000}{S}\right) 10^{L\left(\frac{G}{65,536}-0.5\right)}$$

Each channel was analyzed separately, figure 8 is an example of a line-out on channel 6 (refer to figs 1 & 2). The yellow rectangle is centered over the brightest pixel on the region of interest (ROI) and is 1 pixel high by 20 pixels long. The maximum PSL is immediately given in the ImageJ inset box at the bottom of the image (value = 2.294323). Three corrections are made to the maximum PSL value, fade, background, and normalization to 250J.

Records were kept for the shot time and for the time that the IP is scanned, the fade is calculated using [7]:

$$Fade = 0.347exp\left(-\frac{t}{\tau}\right) + 0.693,$$

t = time from shot to scan, τ = 35:50 [min:sec]

The background was accounted for using the same ROI as the line-out over the spot averaged and subtracted from the PSL value. Finally, each shot was normalized to an energy value of 250J.

To determine the FWHM of the spot the values for each pixel are plotted on an excel chart (fig. 8). The FWHM for this example is 7.2±0.1 pixel, given that each pixel maps to $\frac{25}{3}$μm at the target plane we determine a gross spot size value of 63.33μm. One correction is made to the spot size value, consider the geometry of a point source imaged through a 25μm pinhole. The resultant image on the IP is 100μm corresponding to 100/3 or 33 μm. Thus the net spot size is given by:

$$Spot\ size(net) = \sqrt{(gross\ size)^2 - (33)^2}$$

thus for the example, the final spot size is 50μm.

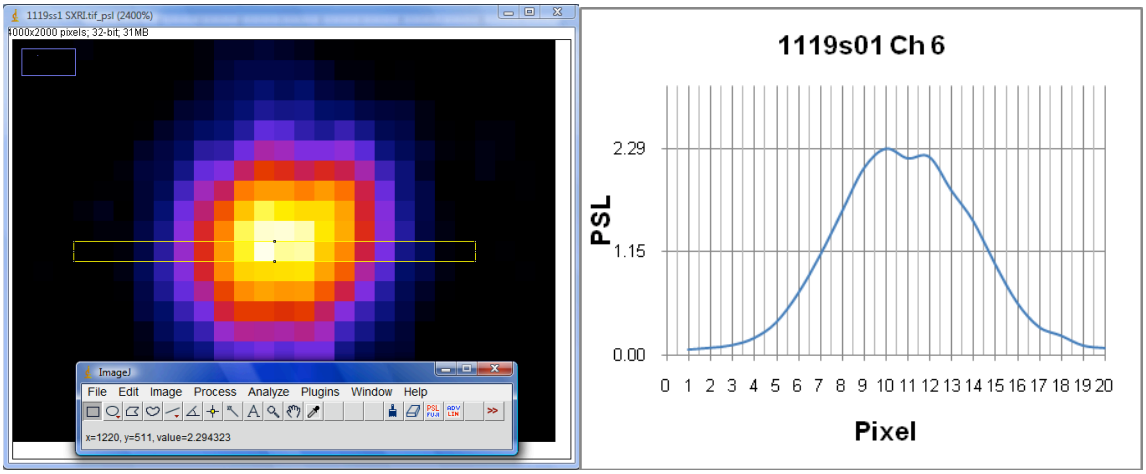

Figure 8: Analysis process; Single channel picture with ROI using ImageJ (*left*), Excel chart showing FWHM (*right*).

In the final analysis each set of data are averaged over identical channels and the error is calculated from both the systematic and standard error.

Experimental setup

The SXRI was one of nearly a dozen used in the 2008 campaigns, the illustration in figure 9 is representative of the final placement configuration. Nearly all of the diagnostics were placed to view the back of the target.

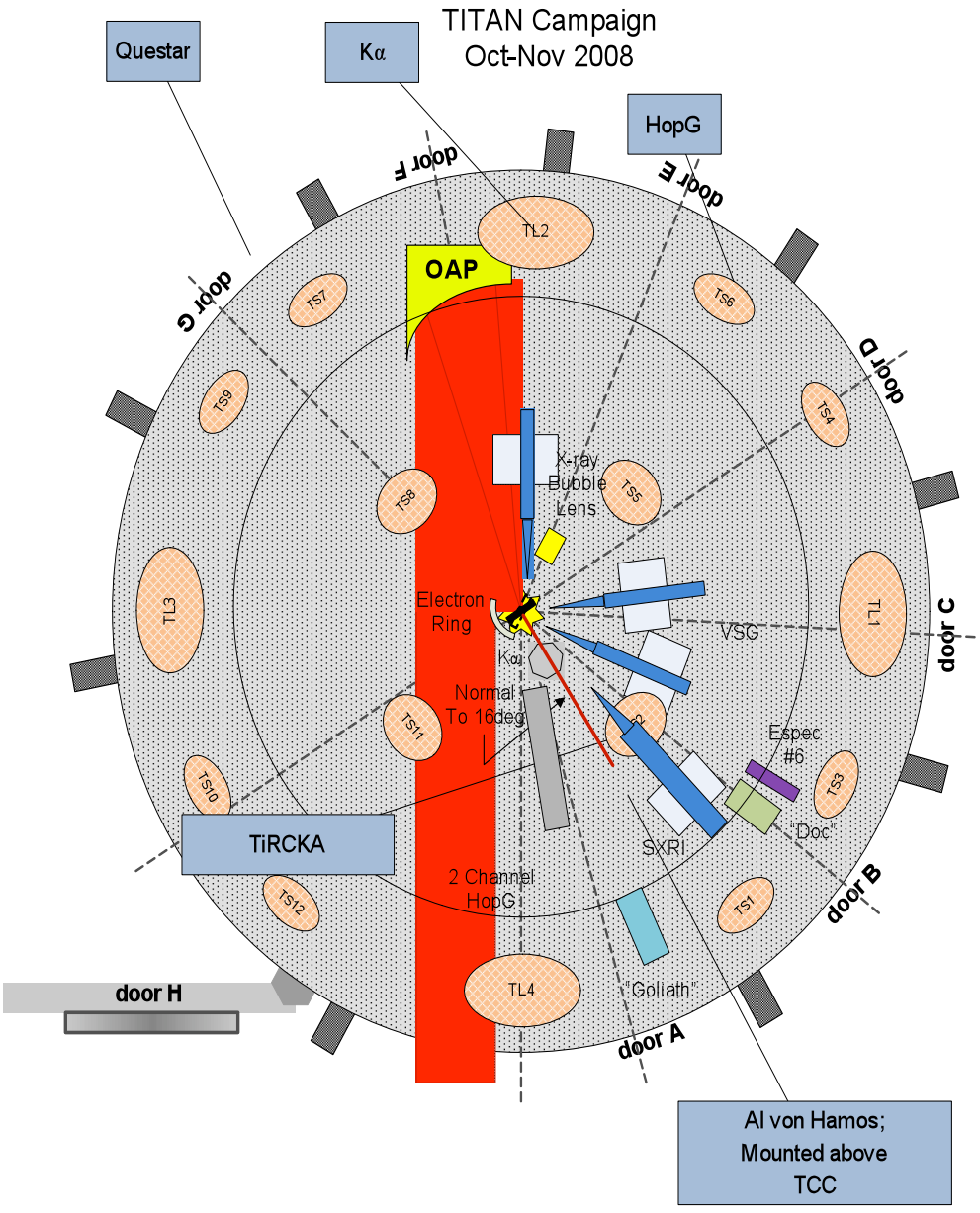

Figure 9: Top view of the Titan target chamber.

Data

During the most recent experimental campaign (Nov. 2008) involving the time-integrated SXRI several systematic studies were performed. These parameter changes included angle of laser incidence, target composition, polarization (S or P), laser pulse length, and induced laser pre-pulse. All the targets were 1mm diameter copper disks of thickness ranging from 2.5 to 5μm. Some were plastic (CH-N) coated faced to the incident beam. A very few had thin aluminum backing to help determine target heating by tamping the back expansion. In all cases the laser wave length was 1064nm (IR). Pulse length ranging from 5-100ps, which affects the maximum intensity of the beam on the target were studied. Finally induced pre-pulse was examined, however the actual level of energy in pre-pulse is in question due to issues with the facilities water cell pre-pulse diagnostic.

The purpose of this study is to find the combination of parameters that produced the highest level of soft x-ray emission over the largest area and minimized the production of higher and lower energy x-rays. The 3X magnification snout was used in this campaign allowing us to take advantage of the straight through central high energy channel. This is described in the previous section and will be referred to as the high pass data. Due to a fortuitous accident in which a section of the filter was broken over the number 15 channel, we were able to monitor the lower energy photon emissions as a pseudo low pass channel. Because the data overlaps the band pass this data will only serve as a reference and not as an absolute number.

In this recent experiment there were 59 usable shots that were divided up into 35 categories, as a result many of the categories only contain a single shot from which to gather data and determine error.

The charts developed and displayed in the following sections are all quite similar in design. In each of the following sections the first chart will generally be a comparison of the three energy bands relative to the maximum PSL count in a given shot. The left vertical axis is scaled for lower values typically found in the soft x-ray and high pass emissions. The left vertical axis is a larger scaling for the low pass emissions. The scaling is not equal from shot to shot so that the data points are easy to examine.

The second chart is a comparison of the soft x-ray PSL count to the soft x-ray spot size. Again primary and secondary axis are used to make the trends in the data easier to discern, with the left vertical axis reserved for the maximum PSL count and the right vertical axis for the FWHM spot size.

In both cases with the charts the title is used to remind the reader of the fixed and variable parameters. The error in this data is determined first from systematic issues in making the measurements from the data sets, then from the multiple channels used in each shot and finally averaged across all the shots within the category (if applicable). Standard error analysis is used [7].

Target Thickness

The first of these studies was across the target thickness parameter. The fixed parameters were as follows; the target was positioned such that the face of the target was 16^0 relative to normal of the incident beam configured in the S polarization scheme, the pulse length was 50ps., no CH-N coating, and the energy was approximately 250J, due to variations in the laser energy delivered by the system, all shot energies were normalized to 250J by multiplying the PSL counts by (250/reported energy). These parameters were chosen because all the available target thicknesses were represented. The 5 μm thick target was a single shot and the data did not register on the IP, however previous experimental campaigns provided evidence that targets with a thickness greater than 4μm did not produce sufficient soft x-rays on the back of the target to register on the IP.

Figure 10 displays the three photon energy bands described previously. The left axis is scaled to the soft x-ray band and the high energy emissions, the right axis the low energy. Both the 3 and 4 μm thick targets have similar maximum PSL levels, and the higher and lower emissions are low relative to the 2.5μm targets.

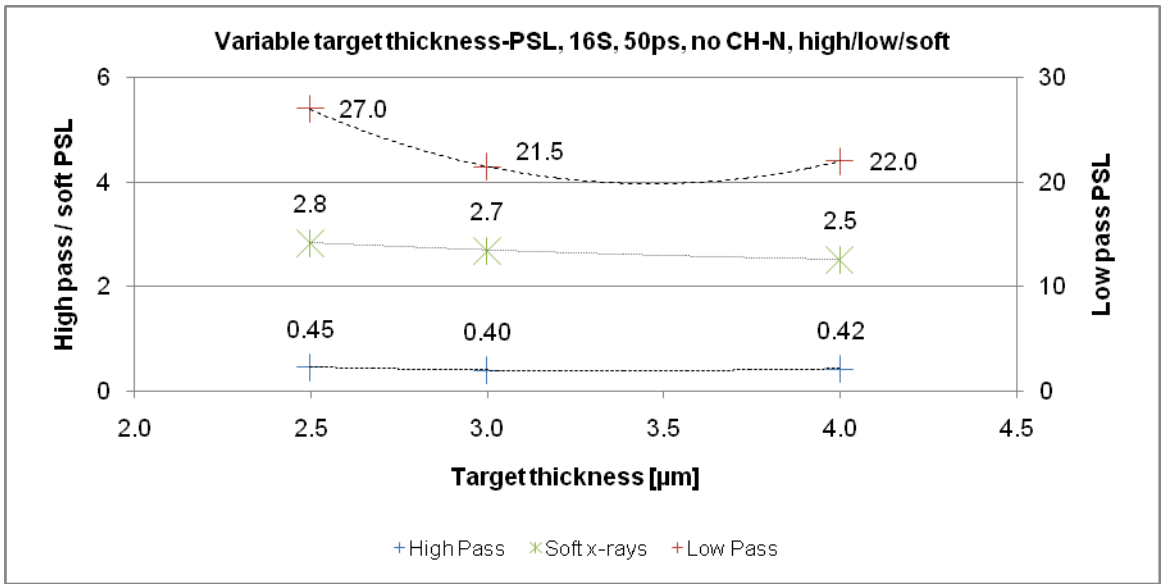

Figure 10: PSL comparison of the High/Low pass and soft x-ray emissions.

The spot size data is represented in figure 11 in comparison to the soft x-ray emissions. The 2.5µm targets have a larger (desired) spot than do the thick targets. This appears to be counter to expected results, standard geometric analysis gives a conical sectioning that has the spot size increase uniformly due to wave front propagation through a solid. Several experiments have been performed in the fast electron (FE) scheme primarily observing the Kα (~8keV) emissions on thin foil and layered targets, there is a significant difference of this experiment from ours, yet there is some data overlap. In these experiments the typical FE propagation angle was measured at 30-50° divergence angle [3,4]. Given these results the 2.5µm targets should have a spot size of 18-21µm, the 3µm thick targets a range of 18.5-22.2µm, and the 4µm thick targets a range of 19.6-24.5µm. Our data supports this for the thicker targets but not for the 2.5µm thick targets.

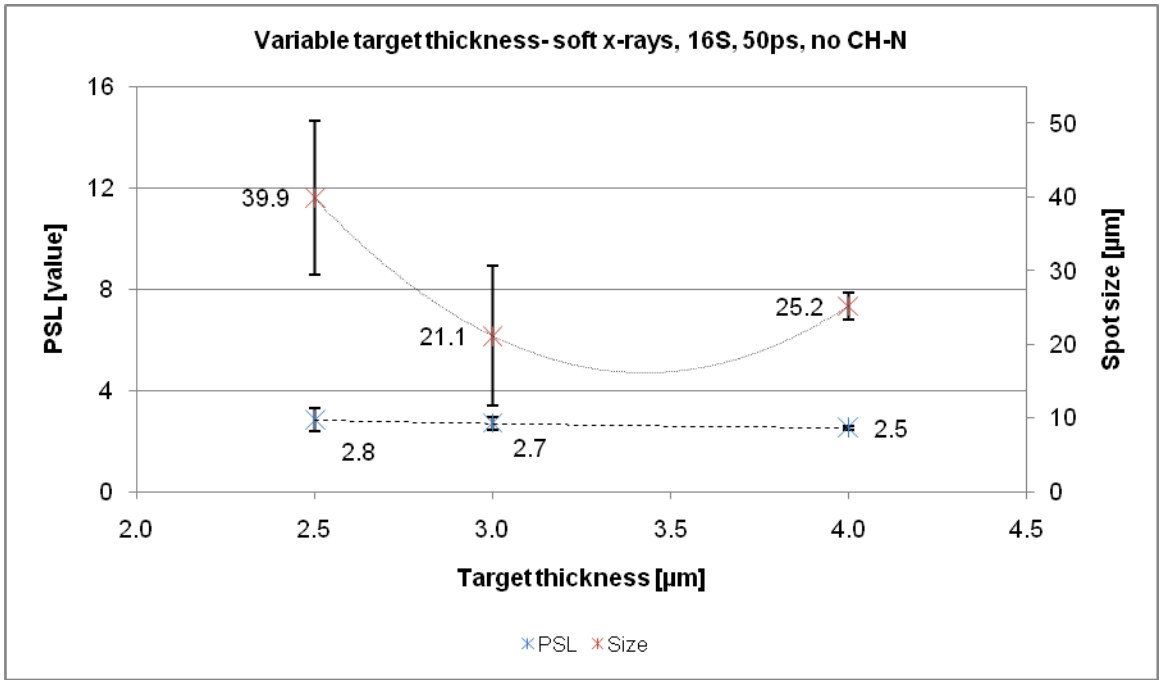

Figure 11: PSL count/ spot size comparison of the soft x-ray channel only for "standard" target.

Experiments performed at the Vulcan and LULI ultra intense laser facilities [5] of the longitudinal electron reflux in a target may give a clue for future experimental considerations.

The second category of the variable target thickness experiments contain two parameter changes, from S to P polarization, and the addition of a thin (1.2µm) CH-N coating. A later section will explore layered target effects and other polarization configurations. Figure 12 is in the same format as figure 10, in this data set there is a significant reduction in the high and low energy PSL count and a lower soft X-ray count for the 4µm thick target.

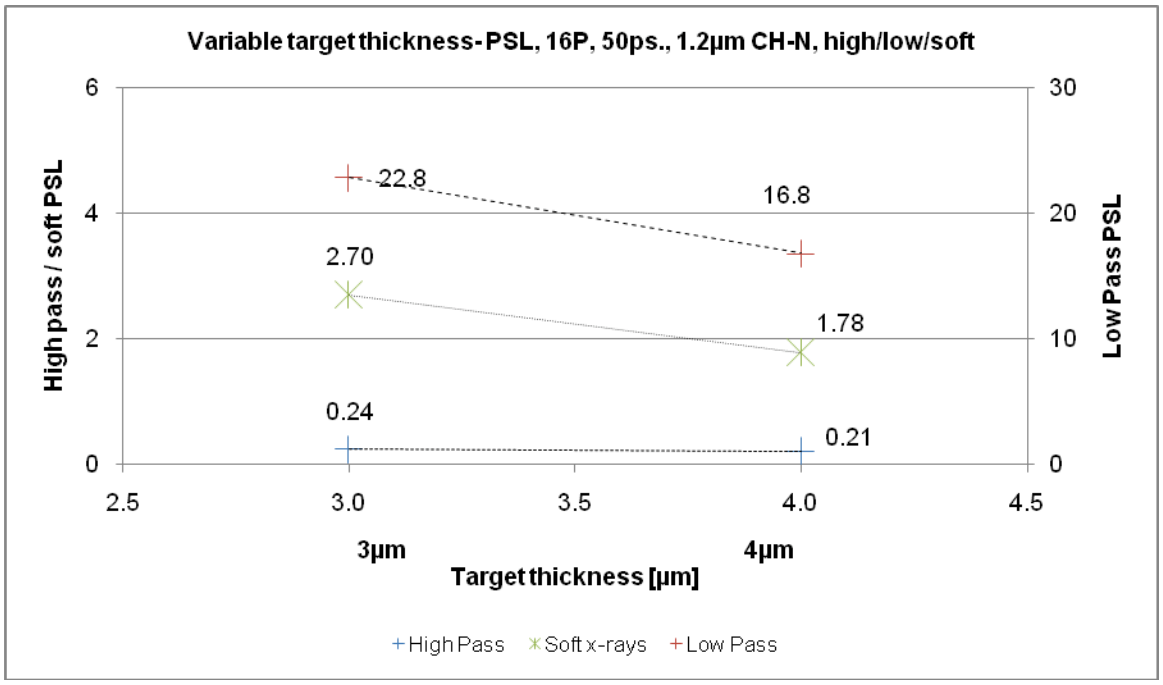

Figure 12: PSL comparison of the High/Low pass and soft x-ray emissions. Polarization of the incident beam is changed from S to P, plastic coating added to absorb laser pre-pulse.

The spot size in the P-polarized plus CH-N configuration is clearly larger the S polarized no CH-N incident angle in figure 13. It is important to note that geometric correction were made to determine the true spot size. In the S polarized configuration the vertical component of the image is true whereas the horizontal is reduced by the cosine of 13^0 (angle of detector relative to target normal back). In the P polarized configuration both the vertical and horizontal axis are not normal to the target, the spot size data was corrected by dividing by the cosine of the polarization angle using a vertical line out. The data from the first category suggests that the true angle of divergence of the FE is 50° {$\theta=\tan^{-1}(y/x)$, x= incident beam size, y=0.5(spot size - x)}. This suggests that a large increase of the spot size for the P-polarized configuration equates to an effective

target thickness an order of magnitude larger than the nominal dimension. These results could be due to the resonance absorption, the factor for P-polarized obliquely incident beams is ~45% greater than for the S-polarized beam given a 16° incidence angle [6].

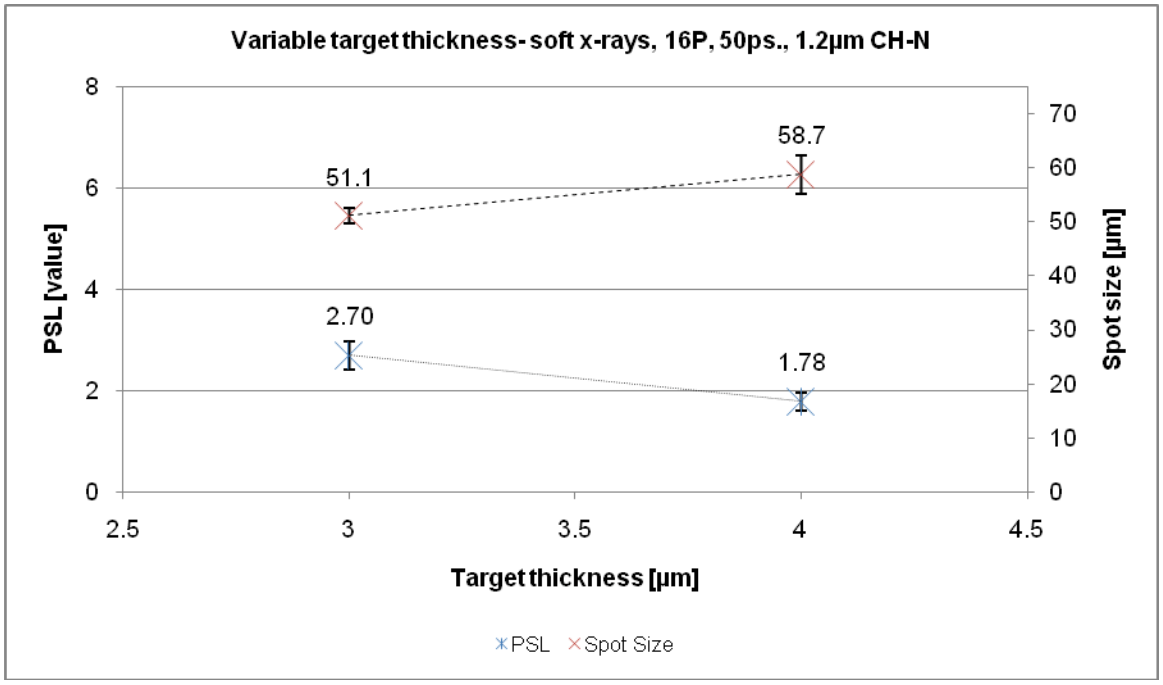

Figure 13: PSL / spot size comparison for soft x-ray channels in P-polarized configuration. Plastic coating on beam side.

Variable Laser Pulse Length

This section of the experiment has the largest sampling and category diversity of the entire campaign. Because of this I am going to change the order of discussion and presented charts. Instead of presenting both charts within each category I will initially examine the high/low/soft PSL for the three categories and follow with by the PSL/spot size comparison.

The first two categories are similar targets with only the incidence angle changed, 3μm thick without plastic coating (figures 14 & 15).

The data in figure 14 confirms previous experimental campaigns our group has performed that showed the ultra high intensity (short pulse length) shots do not produce sufficient soft x-ray emissions to be detected by the IP. At longer pulse lengths the PSL count for the three energy regions increase rapidly at first with the trend flattening at lower intensities.

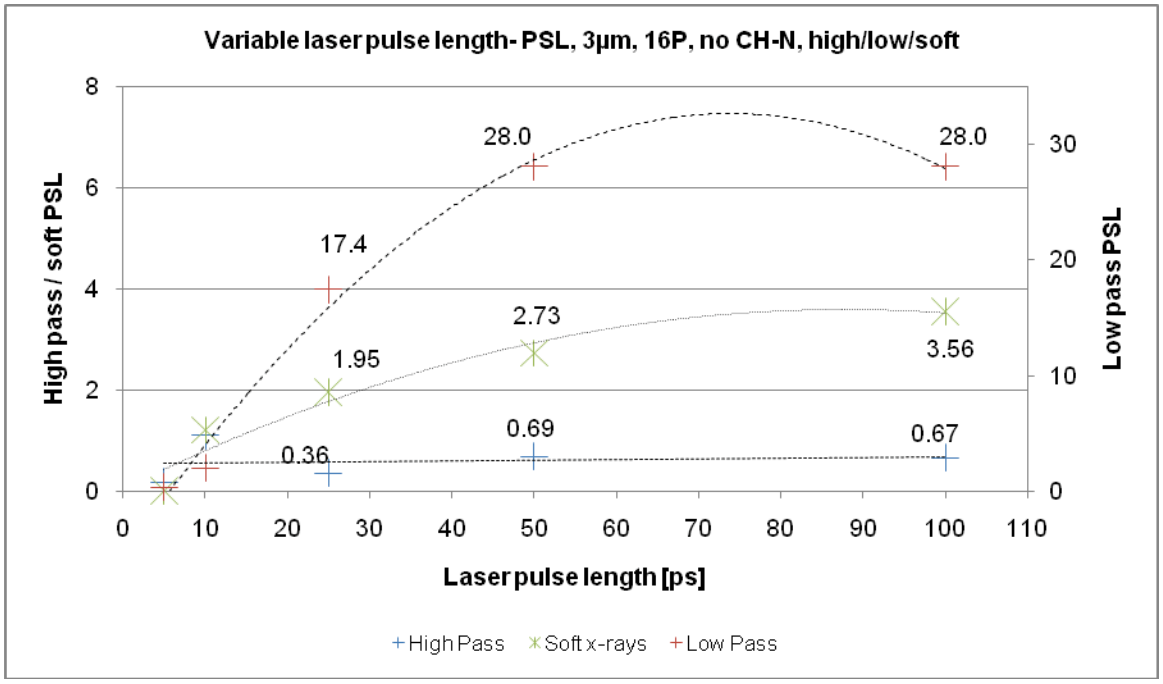

Figure 14: PSL band comparison, 16° P-polarized.

Figure 15 shows a significant drop in all PSL emission values but with similar trends as in figure 14.

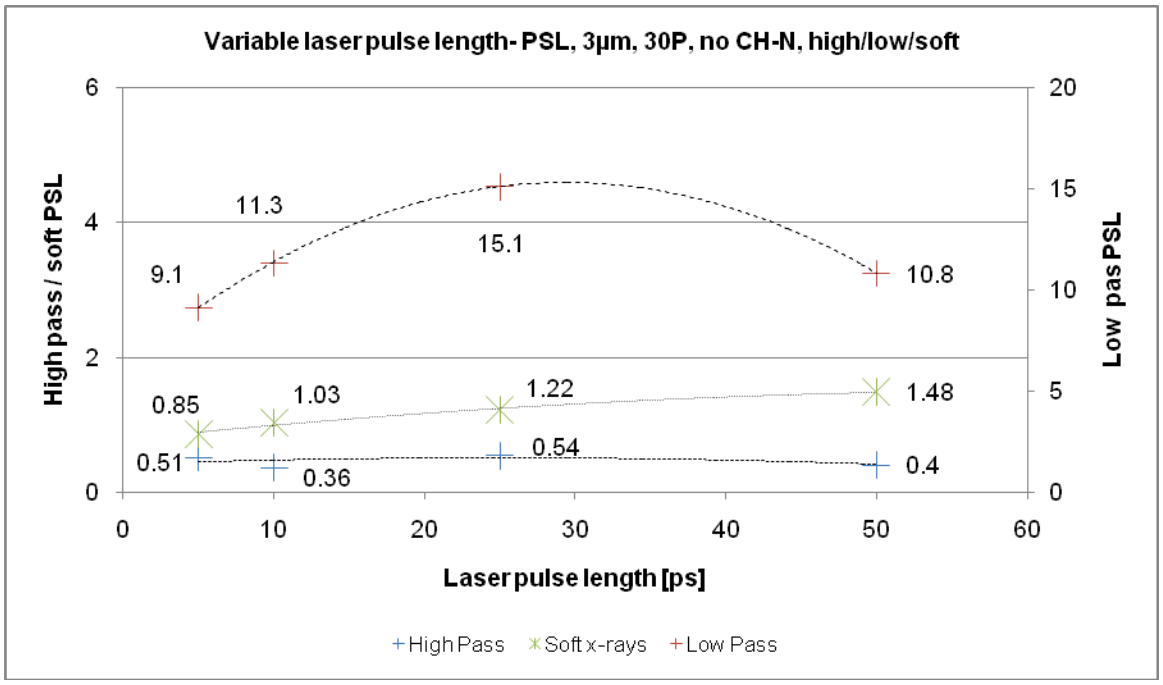

Figure 15: PSL band comparison, 30° P-polarized.

In the third case (figure 16), several parameter factors differ from the previous, the target is thicker with a plastic coating and the polarization is changed from P to S. Also there are only two data sets from which to choose. The low pass signal increase substantially for the 25 ps pulse length and both the maximum soft x-ray and high pass emissions are significantly reduced at the longer pulse length relative to the first category in this sequence.

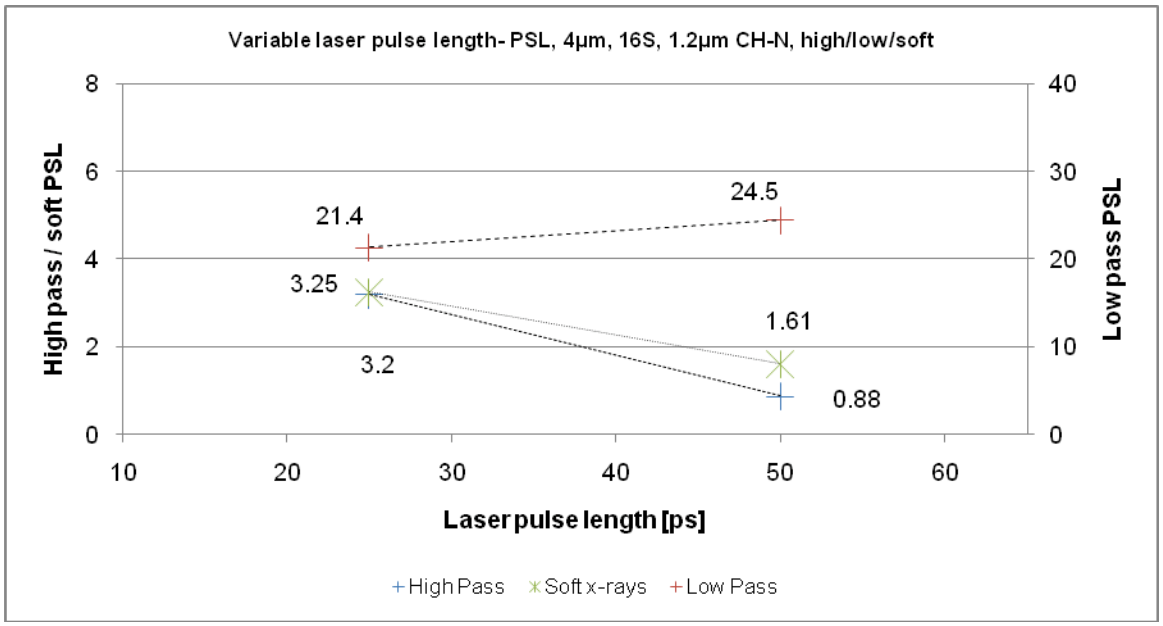

Figure 16: PSL comparison, non standard target, s-polarized.

Figures 17, 18, & 19 show the spot size relative to the soft x-ray PSL count. For all three cases we find that the spot size appears to be at a maximum for the 25 ps pulse length shots and a slight decline and flattening over the longer pulse length shots. However, the PSL count at 25 ps for the P-polarized, 3µm thick targets (figs. 17 & 18) is 40-50% attenuated relative to the long pulse lengths with only a marginal loss in spot size.

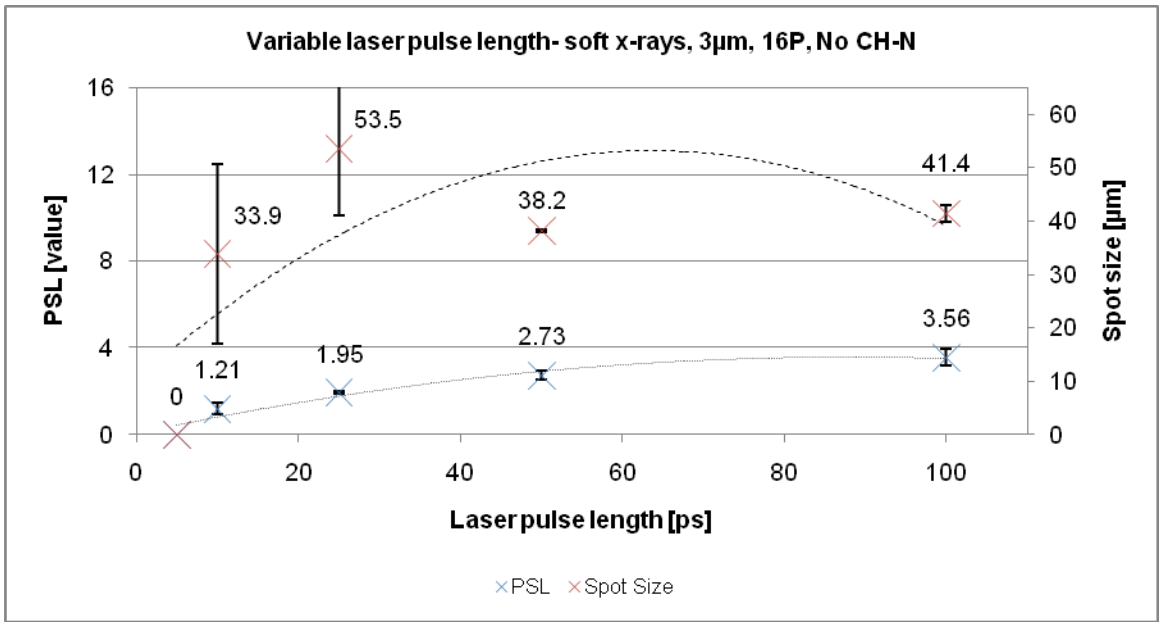

Figure 17: PSL / spot size comparison over changing pulse length. 16° P-polarized.

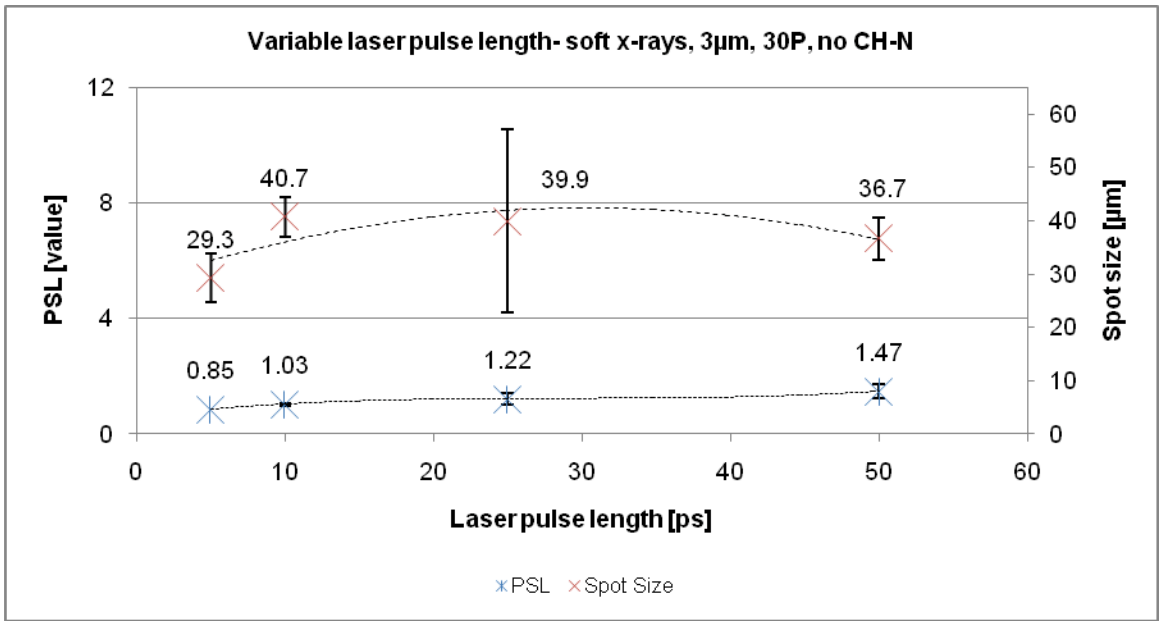

Figure 18: PSL / spot size comparison over changing pulse length. 30° P-polarized.

The PSL/size data for the 4µm thick target shows little spot size change between the 25 ps and 50 ps pulse length with a significant drop in soft x-ray PSL count.

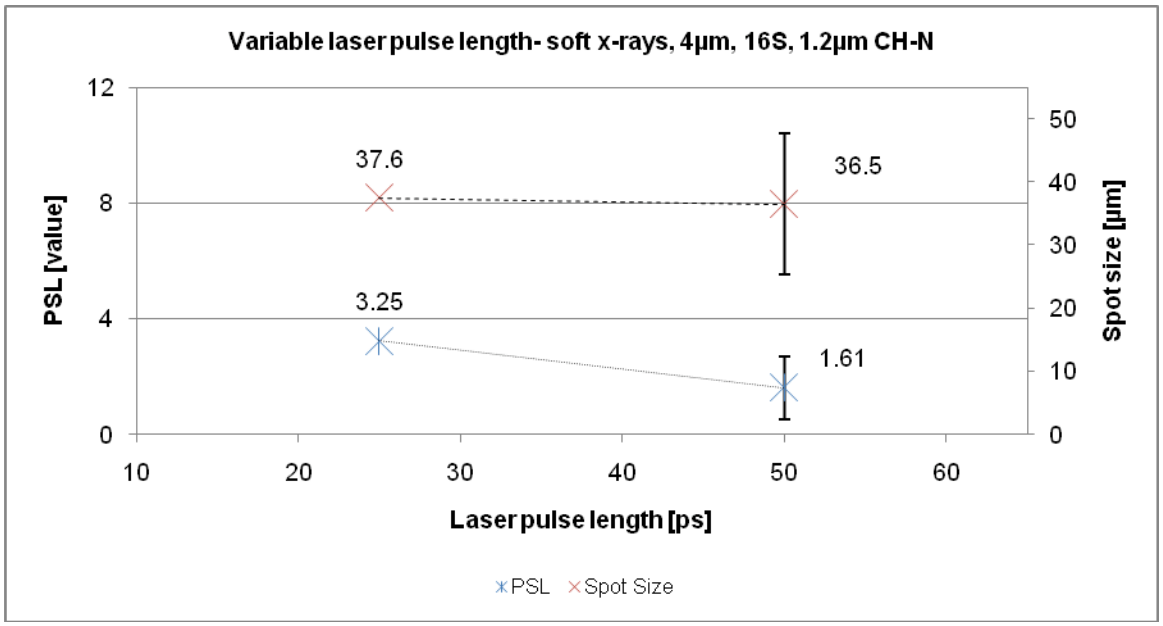

Figure 19:PSL / spot size comparison over variable pulse length. 16° S-polarized, 4µm thick target.

This data suggests that short pulse lengths should be avoided, but more significant results appear to a result of the relative polarization which is discussed in the next section.

Variable Polarization

In the two previous sections one of the factors that seemed to cause a dramatic effect, especially in the spot size, is the polarization of the incident laser beam. In this section we will explore this parameter with two categories of shots. The first of these categories is to compare P to S polarization using a standard target and laser setup, that being 3µm thick target, no coating, mounted at 16° relative to incident beam, and 50 ps pulse length (figs. 20 & 21).

In figure 13 we see that there is no noteworthy difference in the PSL emissions from any of the bands.

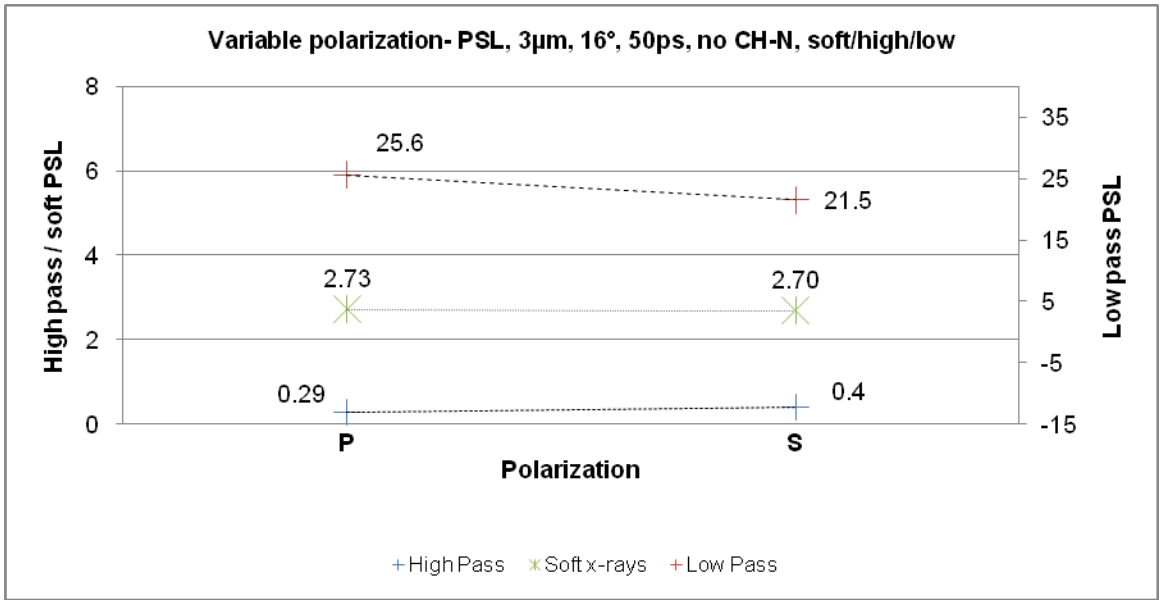

Figure 20: PSL comparison across energy bands, variable polarization, 50 ps pulse length.

Figure 21 gives a vastly different result. The spot size is considerably larger for the P-polarized incident beam as was noted in the previous two sections.

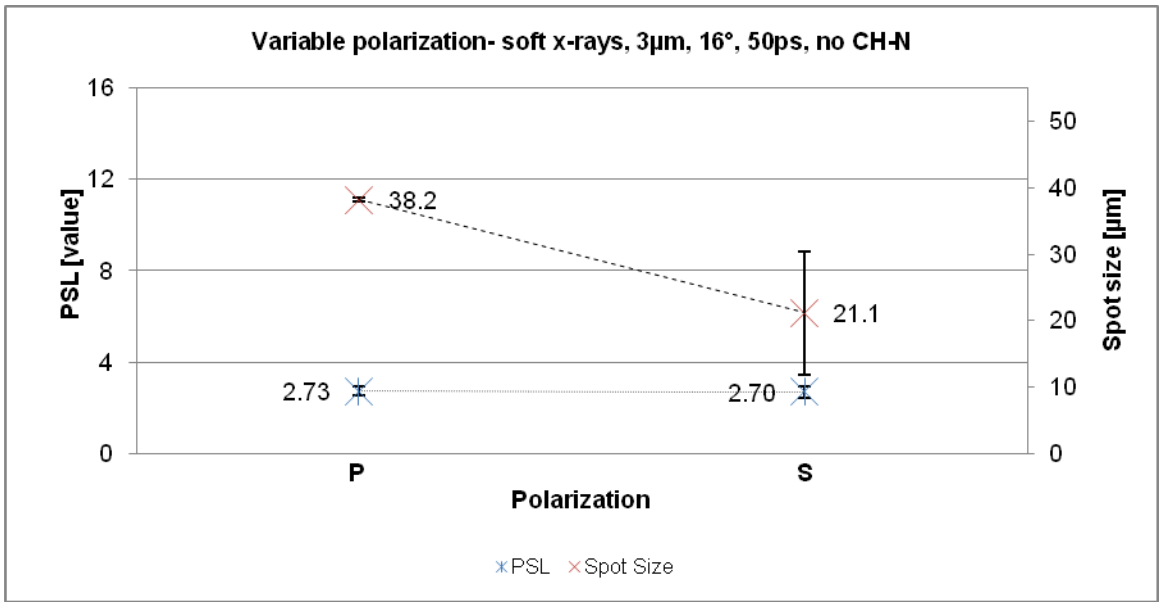

Figure 21: PSL / spot size comparison, variable polarization, 50 ps pulse length.

In the second part of the polarization study a standard target was again chosen, however the pulse length is shortened to 25 ps. This time though a study of a target situated in a P-polarization configuration across a 16°, 30°, and 45° angle of incidence to the beam is the primary concern.

Figure 22 shows a drop off of low pass and soft x-ray PSL emissions from 16° to 30°with a flattening if not rebound at 45°. I find this rebound to be surprising given the early absorption experiments as described by Kruer[5?].

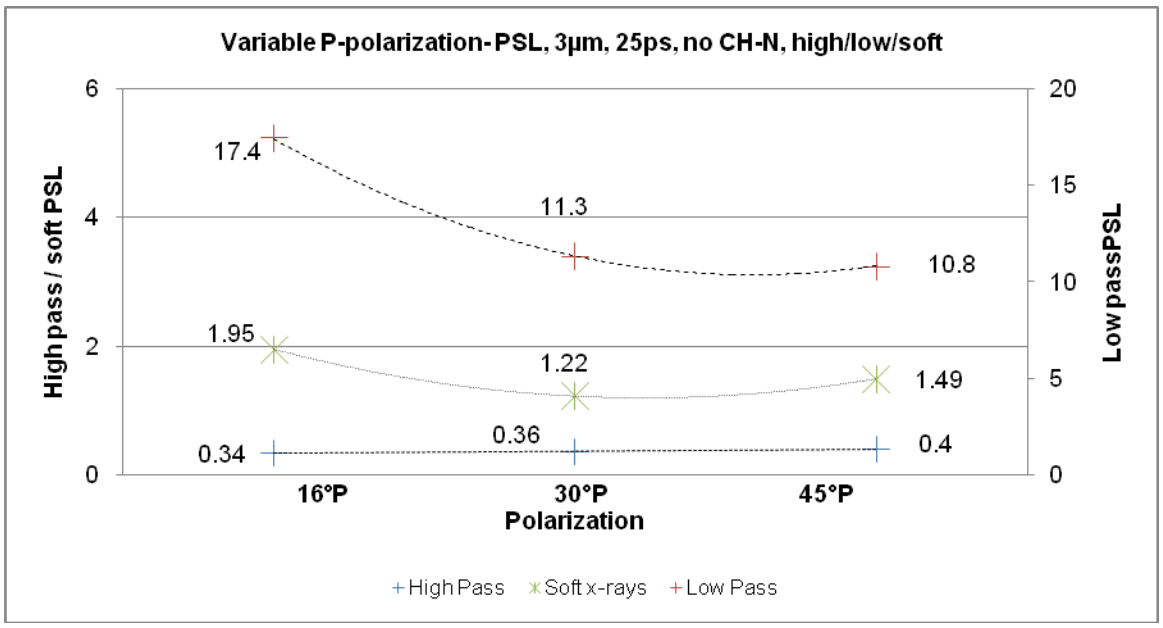

Figure 22: PSL comparison across energy bands, variable relative P-polarization angles, 25 ps pulse length.

The aspect of polarization type and angle of target normal to incidence beam that is most affected is the spot size. The trend is clearly that the spot size decreases uniformly as the relative angle is increased. The results of early experimental work reported in Dr. Kruer's text show that the resonance

absorption of P polarized incident light increases from ~20% at small angles (0° to 10°) up to over 40% at ~22° and then the absorption falls off sharply to 60°. Further experimental configurations where incident angles in between 16^0 and 30^0 should help to determine the possible connection to the absorption properties.

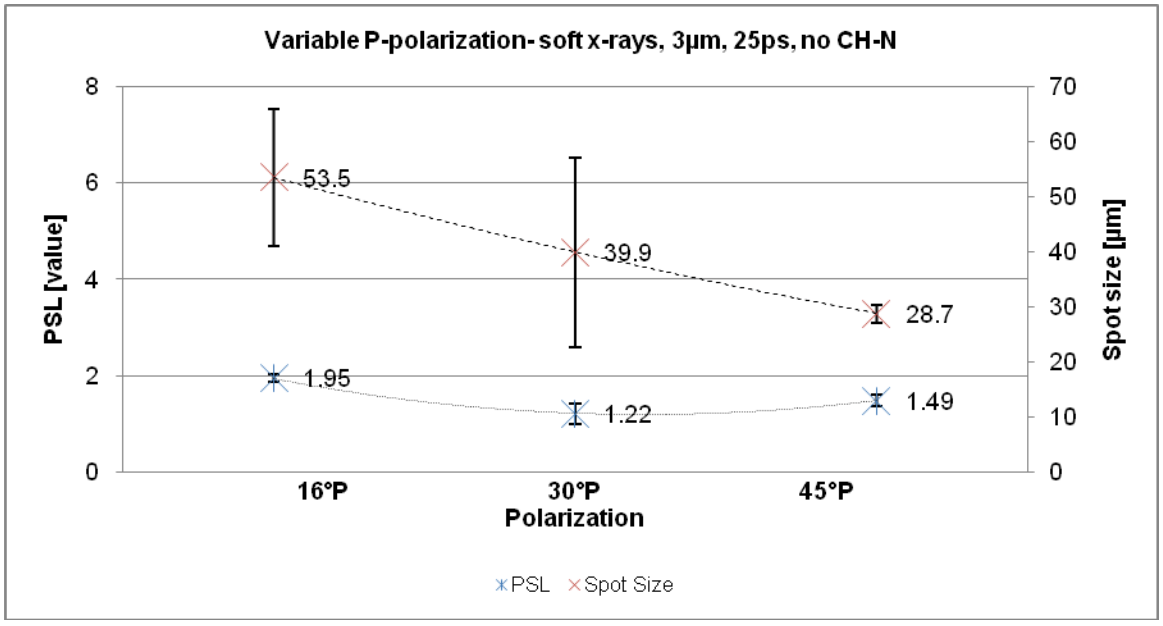

Figure 23: PSL / spot size comparison, variable relative P-polarization angle, 25 ps pulse length.

Induced Pre-pulse

Typically pre-pulse is an undesirable but nearly unavoidable component of the beam profile, measurement throughout the campaign suggest that there is some level of pre-pulse in all the shots with a contrast ratio of 100-500. Two factors generally cause significant pre-pulse, misaligned Pockels cells and applied amplification voltage. In this section of the experiment we induced specific levels of energy in the pre-pulse to determine if there exists a significant

effect on target emissions. The contrast ratio for the induced pre-pulse ranged from 300 to 2700 nominally, however further investigation into the facilities measurement diagnostic (water cell autocorrelation) has come under some doubt as to its accuracy.

Figure 24 shows a small variation in the PSL count for each of the three emission bands. The low pass band emissions are average relative to the entire campaign and the soft x-ray PSL count is in the high end, but the high energy emissions are much larger than any other category.

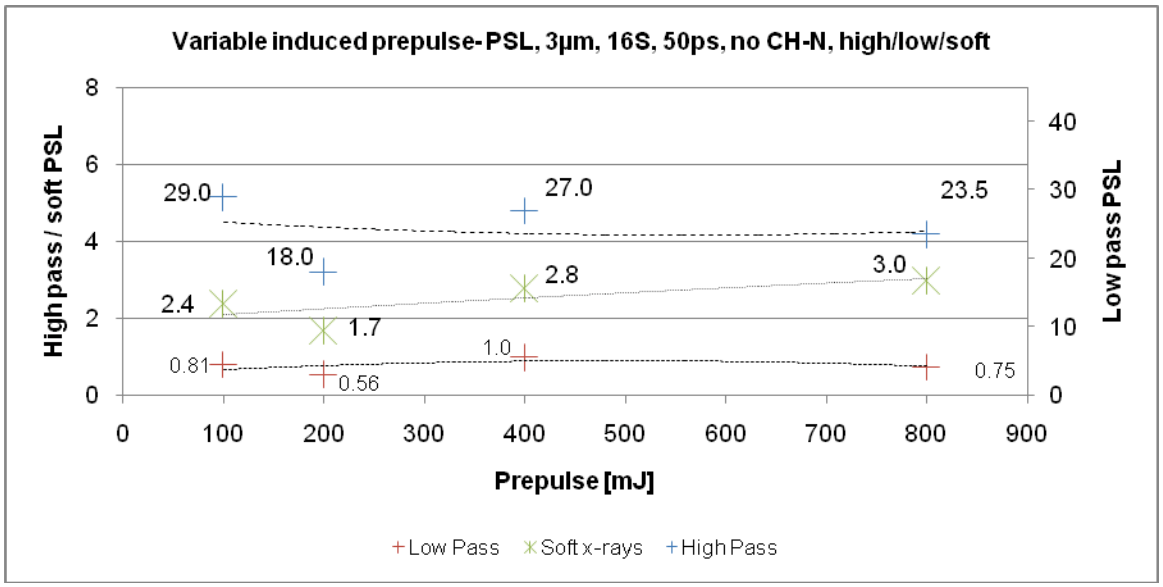

Figure 24: PSL comparison across energy bands, variable induced pre-pulse.

More interesting is the spot size across the parameters, again the deviation from the 100 mJ to 800 mJ shot is small with the exception of the 400 mJ shot which was an under energy shot (fig. 25). In relation to the other categories the spot size is comparable to the 16° P-polarized, 50 ps shots from figure 13. This case differs from the P-polarization case in that the target

thickness is increased due to the expansion of plasma cause by the pre-pulse; when the main beam reaches the interface, the critical surface is moving outward altering the absorption interface position. It could be hypothesized that a configuration of a standard target at 16° P-polarization with a low contrast ratio pre-pulse would give a large spot size and soft x-ray PSL count.

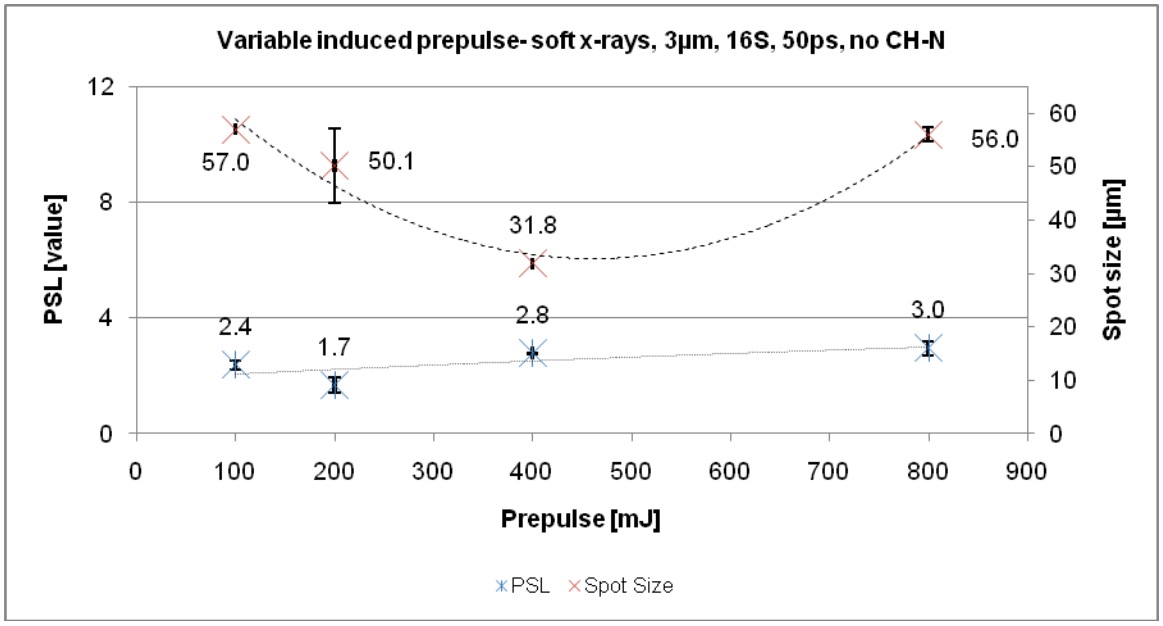

Figure 25: PSL / spot size comparison, variable induced pre-pulse.

Layered Targets

In the final category of this campaign we looked at layered targets. In general we defined layered targets as any copper target either coated on one side or both. The front side layer (facing incident beam) was always a thin plastic coating (CH-N) used to absorb the pre-pulse such that a plasma would not form prior to the arrival of the main beam causing the critical surface to expand

prematurely and thus inhibit the absorption of the laser energy through reflection and instabilities in the preformed plasma.

The Al back on the target is to enhance the 1.4 keV and spectrally shifted Kα emissions [6]. Figure 25 shows a significant increase in soft x-ray emissions for the Al target and an overall flat trend in high and low energy emissions that is on average with the entire experimental data set.

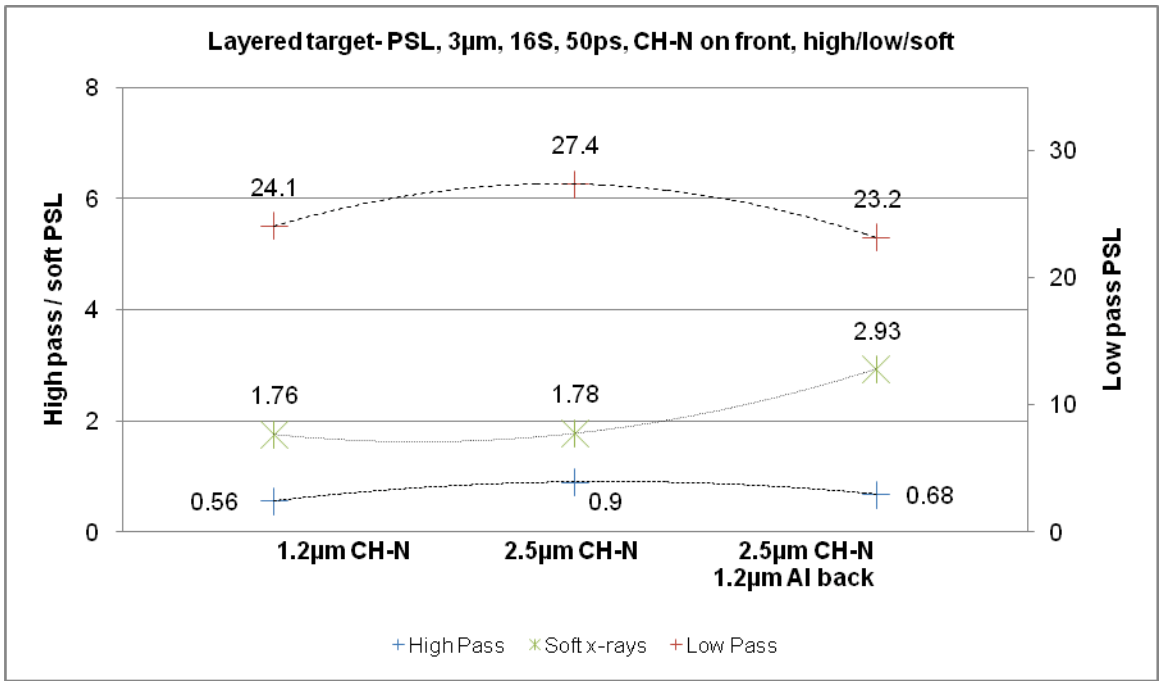

Figure 26: PSL comparison over layered targets. 16° S-polarized.

The final figure (fig. 27) shows a decrease in spot size over the layered targets relative to the induced pre-pulse shots of the previous section. This aspect suggests the CH-N is absorbing most of the non-induced prepulse.

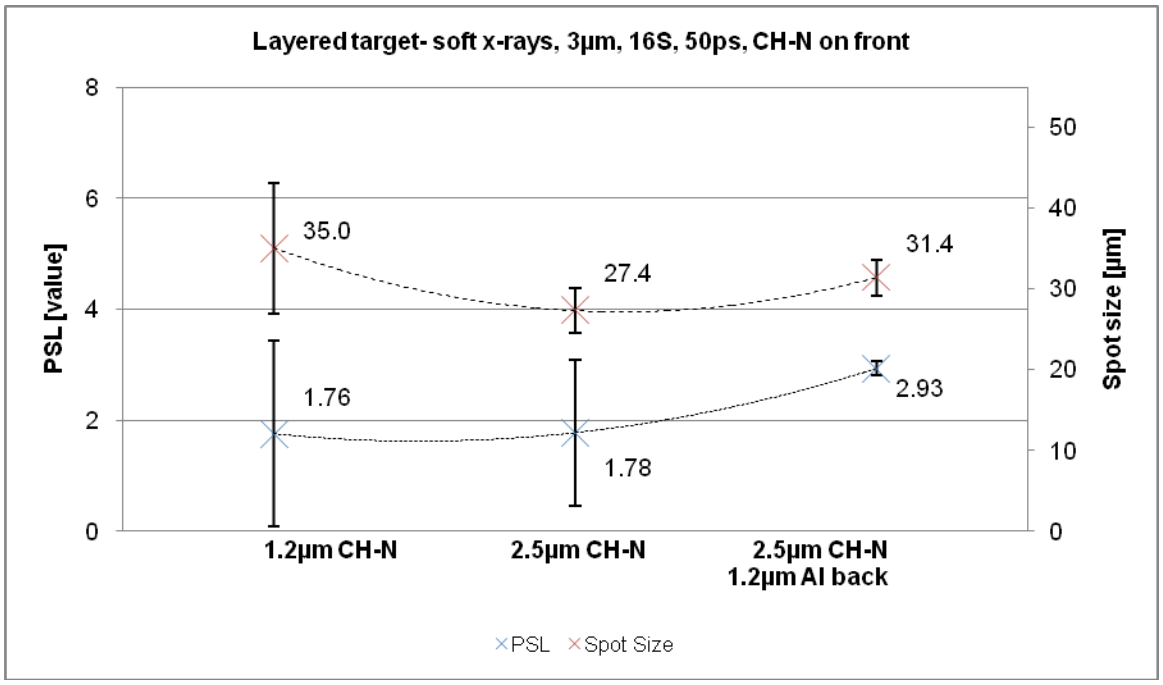

Figure 27: PSL / spot size comparison over layered targets.

Conclusions

The SXRI has proved itself to be not only a robust diagnostic but as a high quality apparatus for future high intensity laser experiments. A second generation SXRI is currently in the development stages for use in NIF. The data in this campaign shows that the SXRI is capable of providing detailed data about the heated region size and x-radiation.

Most of the shots in this campaign exhibit small error, those in which the error is large does present a degree of concern. Much of the error stems from a variety of sources. Some of the largest error are from combinations of shot which were taken during the first few days of the experiment when the SXRI diagnostic was not fully aligned. The normalization method also created some significant error primarily in the PSL count for the variable pulse length category. Other

factors that lead to exaggerated error were the chart scaling, inconsistencies in the target surface, and target alignment. Even though the fitted trend lines were intended purely as a visual reference, the correlation to fit was nearly or exactly 1 for all of the second order curved lines.

References

[1] M.B. Schneider *et al*., UCRL-CONF-221117 (2006).

[2] David Balihar, http://www.pinhole.cz/en/pinholecameras/whatis.html

[3] R. Kodama, *et al*., Nature **412**, 798 (2001).

[4] J.J. Santos *et al*., Phys. Rev. Letters **98** 025001 (2002)

[5] M. Nakatsutsumi *et al*., Journal of Physics: Conference Series **112** (2008) 022063.

[6] E. Martinolli *et al*., Physical Review E **73**, 046402 (2006).

[7] A.L. Meadowcroft, C.D. Bentley, E.N. Stott, *Characterization of an image plate system for x-ray diagnostics.* AWE/PPDG/08/ALM/061 (2008).

[8] C.H. Aedy, K.I. Parker, *Characteristics of MS image plates and Fuji BAS 2500 image plate scanner (2),* AWE/HD01/B/0302/413 (2003)

[9] K.I. Parker, *Characterization of the Fuji FLA7000 image plate scanner,* AWE/HD02/B/0801/78 (2008)